Aerodynamics for the ADEPT SR-1 Flight Experiment

Ashley M. Korzun* and Soumyo Dutta†
NASA Langley Research Center, Hampton, VA, USA

Ryan D. McDaniel‡
NASA Ames Research Center, Moffett Field, CA, USA

Christopher D. Karlgaard§ and Jake A. Tynis¶
Analytical Mechanics Associates, Inc., Hampton, VA, USA

Adaptable, Deployable, Entry, and Placement Technology (ADEPT) is a combination of a heatshield and an aerodynamic decelerator for atmospheric entry applications. The ADEPT Sounding Rocket (SR)-1 mission was a suborbital flight experiment of an 0.7 m-diameter ADEPT to verify system-level performance and to characterize dynamic stability behavior. The aerodynamic database for ADEPT SR-1 was constructed from non-continuum and continuum flowfield computations, along with data from recent ADEPT ground testing and the IRVE-3 flight test vehicle. High-altitude (free-molecular and transitional regimes) data were generated using DSMC methods. Pre-flight predictions of continuum static aerodynamics coefficients were derived from Reynolds-Averaged Navier-Stokes solutions at conditions along a design trajectory, with comparisons to available ground test data of the nano-ADEPT geometry. Dynamic pitch damping characteristics were taken from functional forms developed for the IRVE-3 flight test vehicle through ballistic range testing. Comparison of pre-flight predictions to post-flight reconstruction of aerodynamic force and moment coefficients is presented.

I. Introduction

Adaptable, Deployable, Entry, and Placement Technology (ADEPT) is an aerodynamic decelerator to enable missions to planetary bodies with atmospheres. Deployable decelerators are beneficial where the stowed volume of the entry vehicle limits the drag area attainable with a traditional, rigid aeroshell. ADEPT is an exo-atmospherically deployed, rigid-ribbed structure covered with 3D-woven carbon fabric that significantly increases the drag area of the entry vehicle, which lowers the vehicle's ballistic coefficient and reduces the severity of aerothermodynamic environments in flight [1, 2].

The ADEPT Sounding Rocket (SR)-1 flight experiment was the first flight of a nano-ADEPT system [1, 2]. The successful launch, flight, and recovery occurred on September 12, 2018 at White Sands Missile Range, New Mexico. The test objectives for ADEPT SR-1 were to demonstrate exo-atmospheric deployment and supersonic/transonic stability without active control in atmospheric flight. The key performance parameters and mission success criteria are listed in Table1.

The concept of operations for the flight experiment is shown in Fig. 1. ADEPT SR-1 launched from Spaceport America on a SpaceLoft XL (UP Aerospace) sounding rocket with a target payload apogee of 115 km. Following de-spin and nose cone separation, the ADEPT payload was jettisoned from the sounding rocket in the stowed configuration. The heatshield was deployed near apogee, maintaining the nominal spin rate for entry of 40 deg/s. ADEPT SR-1 then decelerated upon re-entering the atmosphere, targeting a peak Mach number of 3 and stable deceleration down to Mach 0.8 conditions. No active control or additional decelerator devices were used, and the test article impacted the ground at 25 m/s approximately 15 minutes after launch. All data were stored onboard the vehicle and recovered post-flight. Additional details on ADEPT SR-1 test objectives and concept of operations have been described in earlier publications [1, 2]. The objective of this work is to summarize the aerodynamics database used in both pre-flight and post-flight analysis of ADEPT SR-1 flight performance.

*Research Aerospace Engineer, Atmospheric Flight and Entry Systems Branch, M/S 489, Member AIAA.
†Aerospace Engineer, Atmospheric Flight and Entry Systems Branch, M/S 489, Member AIAA.
‡Research Scientist, Aerothermodynamics Branch, M/S 230-2, Senior Member AIAA.
§Supervising Engineer, Atmospheric Flight and Entry Systems Branch, M/S 489, Senior Member AIAA.
¶Aerospace Engineer, Atmospheric Flight and Entry Systems Branch, M/S 489, Member AIAA.

Table 1 ADEPT SR-1 test objectives summary

Key Performance Parameters		
Performance Parameter	Threshold Value	Project Goal
Exo-atmospheric deployment to an entry configuration of the 1m-class ADEPT.	Less than fully locked condition resulting in shape with less than 70° cone half-angle.	Full, locked deployment before reaching 80 km altitude on descent, to 70° cone half-angle achieving 6x greater drag area.
Aerodynamic stability without active control of the 1m-class ADEPT in a flight configuration.	Does not tumble prior to $M_\infty = 0.8$ while decelerating from peak Mach number.	ADEPT does not tumble before ground impact; Sign of pitch damping coefficient (C_{mq}) is determined; FF-CFD simulation tool is validated

Mission Success Criteria	
A	ADEPT separates from the sounding rocket prior to apogee.
B	ADEPT does not re-contact any part of the launch vehicle after separation.
C	ADEPT reaches an apogee greater than 100 km.
D	ADEPT achieves fully deployed and locked configuration prior to reaching 80 km altitude.
E	Obtain on-board video of deployed ADEPT to observe fabric response and flight dynamics during entry.
F	Obtain data necessary to reconstruct ADEPT 6-DOF descent trajectory to ***required accuracy below*** with 95% confidence from Mach 3.0 while decelerating to ground impact: a. Mach number: 0.1 b. Drag coefficient: Larger of 5% or 0.005 c. Total angle of attack: 2° (if not tumbling) d. Sign of pitch damping sum

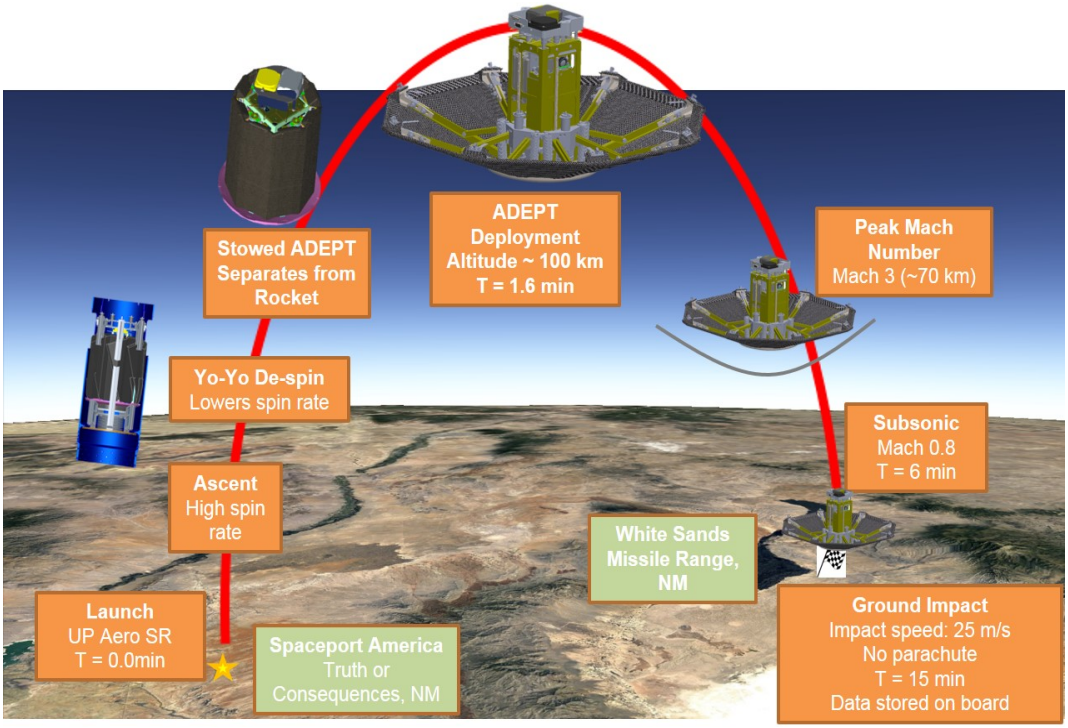

Fig. 1 ADEPT SR-1 concept of operations.

II. Background

The following sections describe the ADEPT SR-1 flight test article, design trajectory, aerodynamics database structure, computational methods, and uncertainties applied in Monte Carlo trajectory simulations.

A. Test Article Geometry and Design Trajectory

The deployed ADEPT SR-1 geometry, shown in Fig. 2, was an eight-sided, faceted cone with a 70° half-angle and a spherical nose segment. The deployable heatshield, with an exposed payload and aft structure, is similar to that of the hypersonic inflatable aerodynamic decelerator (HIAD) test articles flown on the IRVE-II and IRVE-3 missions [3, 4], where the IRVE geometries were 60° sphere-cone forebodies with a maximum diameter of 3.0 m (see Fig. 2), and ADEPT SR-1 was a 70° faceted sphere-cone with a maximum diameter of 0.6878 m (measured rib tip to rib tip). The reference area, 0.3716 m, was defined by a circle having this diameter. The payload was a 3U CubeSat. Additional details on the ADEPT SR-1 geometry are provided in Fig. 3. The axial center of gravity (CG) position for ADEPT SR-1 was at a distance x_{CG}/D of 0.15, aft of the nose. While this CG position is further forward than is typical of blunt body entry vehicles, this position was chosen explicitly to have the vehicle impact the ground nose-first, in order to protect the flight data stored onboard the payload. With an entry mass of 11 kg, ADEPT SR-1 had a ballistic coefficient of approximately 20 kg/m^2 ($C_D \approx 1.5$). The aerodynamics data sets, methods, tools, and implementation applied to ADEPT SR-1 draw from experience on the IRVE missions [3, 4].

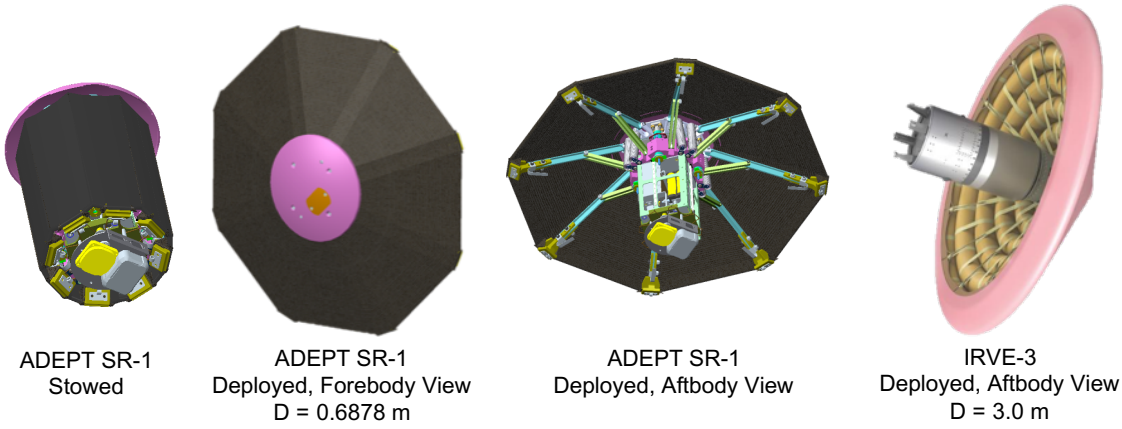

Fig. 2 ADEPT SR-1 and IRVE-3 flight test articles.

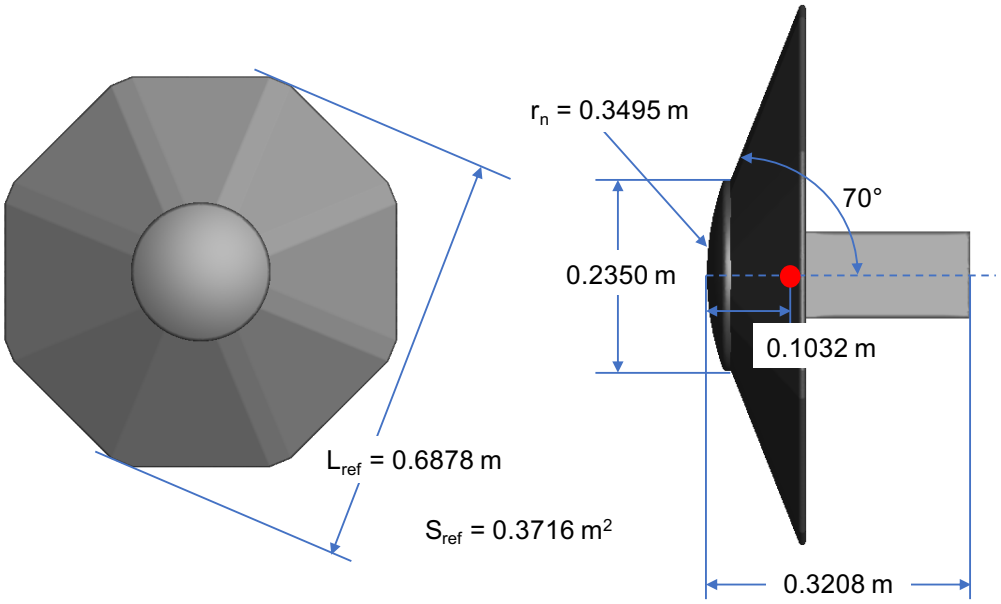

Fig. 3 ADEPT SR-1 geometry.

Forebody geometry generally dominates blunt body aerodynamics at hypersonic conditions, with aft geometry contributing progressively more at supersonic and subsonic conditions due to increasing base pressure coefficient with decreasing Mach number. The altitude-velocity profile and atmospheric density also govern the resulting aerodynamics. A design reference trajectory was used to specify atmospheric conditions for aerodynamics analysis. The design trajectory targeted a minimum separation altitude of 100 km for ADEPT SR-1 and a peak Mach number during entry of 3.0. The design trajectory is shown in Fig. 4. Atmospheric interface was defined at 85 km (above mean sea level).

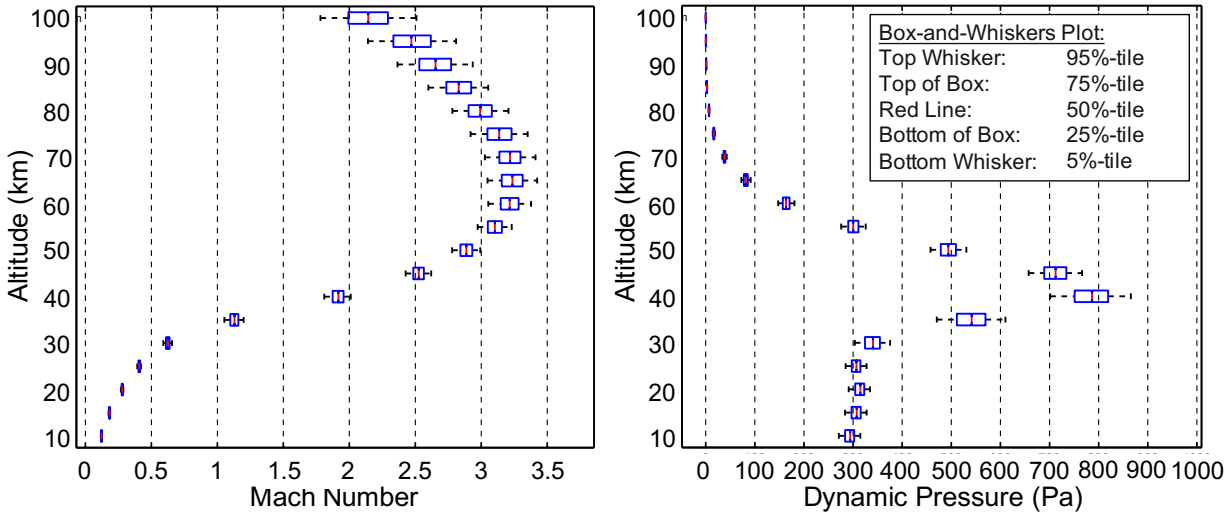

Fig. 4 ADEPT SR-1 design trajectory.

B. Static Aerodynamics

The ADEPT SR-1 aerodynamics database (ADB) structure and methods were based on those developed for the successful Earth-based IRVE-II and IRVE-3 flight experiments [3–5] as well as the Mars Exploration Rovers and Phoenix Mars entry capsules [6, 7]. As described in Table 2, the ADB was organized by flight regime, with inputs of angle of attack, angle of sideslip, Knudsen number, and Mach number. The aerodynamic coordinate system is given in Fig. 5.

Table 2 Static aerodynamics flight regimes and data methods

Flight Regime	Range	Input Parameters	Method
Free-Molecular	$Kn > 100.63$, $0° \leq \alpha_T \leq 180°$	α, β	DAC [8]
Transitional	$0.0104 \leq Kn \leq 100.63$, $0° \leq \alpha_T \leq 180°$	α, β, Kn	DAC [8] , MAP [9]
Supersonic	$Kn < 0.0104$ and $M_\infty > 1.0$, $0° \leq \alpha_T \leq 20°$	α, β, M_∞	US3D [10, 11]
Subsonic	$M_\infty < 1.0$, $0° \leq \alpha_T \leq 20°$	α, β, M_∞	FUN3D [12, 13]

The ADB presented here assumed the vehicle to be axisymmetric. This assumption allowed the aerodynamic coefficients to be specified in the total angle of attack plane and then decomposed into the α and β planes for use in a 6-DOF trajectory simulation. Total angle of attack, α_T, shown in Fig. 5 above, is defined in the plane of the vehicle's velocity and axial symmetry axis. This axis was arbitrarily chosen for ADEPT SR-1 to bisect a single gore on the heatshield. As the number of gores increases, the forebody shape approaches that of a smooth sphere-cone. It was unknown prior to the flight if the eight-gore, faceted geometry of ADEPT SR-1, when spin-stabilized, would approximate a truly axisymmetric blunt body.

It was assumed that the vehicle was rigid, with negligible mid-gore deflections during flight. An aerodynamic loads test was completed in April 2015 at low subsonic conditions ($M_\infty < 0.3$) to obtain static deflected shape data and pressure distributions on an 0.7 m-diameter ADEPT article across a range of fabric pre-tensions, dynamic pressures,

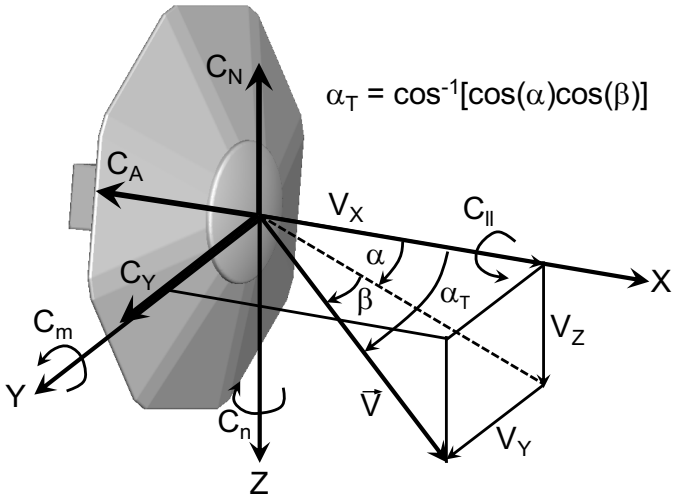

Fig. 5 ADEPT SR-1 aerodynamics coordinate frame.

and angles of attack, in addition to force and moment balance data [14]. The requirement on ADEPT SR-1 for the maximum deflection was $\delta/L_{gore} \leq 0.02$. At the targeted fabric pre-tension and maximum dynamic pressure expected for ADEPT SR-1, the measured δ/L_{gore} in this static loads test was 0.005. This amount of deflection yields a projected area equal to 99.5% of that for an ideal 70°, 8-sided pyramid. On the basis of this result, the ADB assumed ADEPT SR-1 to behave as a rigid heatshield and did not account for any mid-gore or rib deformation.

Static aerodynamic coefficients were tabulated at multiple points along the design trajectory (Fig. 6) using the methods listed in Table 2 for α_T values of 0°, 10°, and 20°. This range of α_T was chosen to bound the expected angle of attack and sideslip envelope in flight for a ballistic blunt body with no active control. The upper limit of 20° bounds reconstructed angles of attack and sideslip from both IRVE-II (spinning, no active control) [3] and Phoenix (not spinning, reaction control system dead-banded in the atmosphere) [7]. Note that in Fig. 6, an earlier iteration of the design trajectory with a lower apogee was used to generate the non-continuum portion of the ADB. Aerodynamic coefficients were linearly interpolated between flight regimes, and all moments were reported about the nose (heatshield center).

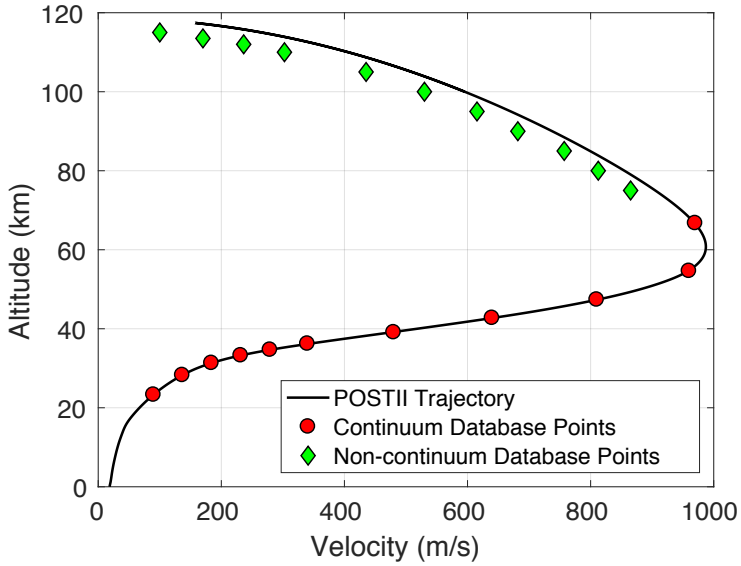

Fig. 6 Static aerodynamics anchor points along the ADEPT SR-1 design trajectory.

The non-continuum aerodynamics were predicted using a computational methodology that accounts for interactions amongst individual molecules and between individual molecules and the vehicle. Free-molecular data originally generated for IRVE-3 with the direct simulation Monte Carlo (DSMC) analysis code (DAC) were used for Kn > 2.23 (115 km) [4, 8]. Transitional data were generated for the ADEPT SR-1 geometry at altitudes from 115 to 75 km (Kn = 2.23 to 0.0023) with the MAP [9] (lower density conditions) and DAC [8] (higher density conditions) codes and included in the ADB to bridge the free-molecular and continuum flow regimes.

The suborbital flight resulted in peak Mach numbers corresponding to supersonic conditions. With no supersonic wind tunnel test data available for the ADEPT SR-1 faceted geometry, the continuum, static aerodynamics were based entirely on computational fluid dynamics (CFD) simulations. Supersonic and transonic conditions were simulated using the US3D code [10, 11], and subsonic conditions were simulated using the FUN3D [12, 13] code. While the flight experiment ends at Mach 0.8, solutions were computed down to Mach 0.3. In all cases, forces and moments were computed on both forebody and aftbody surfaces.

1. Supersonic Static Aerodynamics CFD Simulation Approach

Supersonic static aerodynamics were generated with the Unstructured Three-Dimensional (US3D) CFD code [10, 11]. US3D is an implicit and parallel flow solver of the compressible, finite-volume Navier-Stokes equations on both structured and unstructured meshes. The code also includes modeling options for solving complex flows with effects of finite-rate chemistry and thermal nonequilibrium, neither of which needed to be modeled for ADEPT SR-1. For the cases presented here, convective fluxes were computed using a 2nd order Modified Steger-Warming flux vector splitting method with a MUSCL scheme using a pressure limiter. Time integration was performed with the implicit 2nd order DPLR [15] method where wall normal lines exist. Full matrix point relaxation was used everywhere else in the domain. The freestream was modeled with calorically perfect air, and the viscosity was computed using Sutherland's law. The flow was assumed to be fully turbulent and was modeled using the Spalart-Allmaras turbulence model with the Catris-Aupioux compressibility correction.

The grid for the US3D solutions was generated on a simplified geometry that eliminated the struts on the backside of the heatshield. The ribs that support the heatshield fabric were included in the grid geometry. The CubeSat payload was simplified to a smooth, 3U box. Although US3D can accept unstructured grids, a fully structured grid was used for ADEPT SR-1 aerodynamic database solutions to allow for checks against solutions generated with the DPLR CFD code [15]. The half-body grid with a symmetry pitch plane contained 11.8 million points. Figure 7 shows the half-body geometry and grid topology. All US3D results were rotated to account for the differences in coordinate frame to agree with the definition given in Fig. 5.

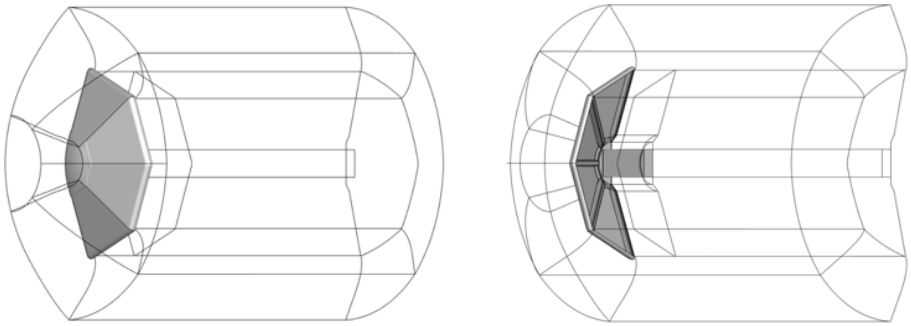

Fig. 7 US3D geometry and structured grid topology.

Figure 8 shows Mach number and pressure contours for a Mach 3.0 case. As expected, the supersonic CFD solutions were unsteady, due to the separated wake flow aft of the maximum diameter. The aerodynamics of the vehicle were dominated by the forebody pressures, which were an order of magnitude greater than those on the backside, including fluctuations.

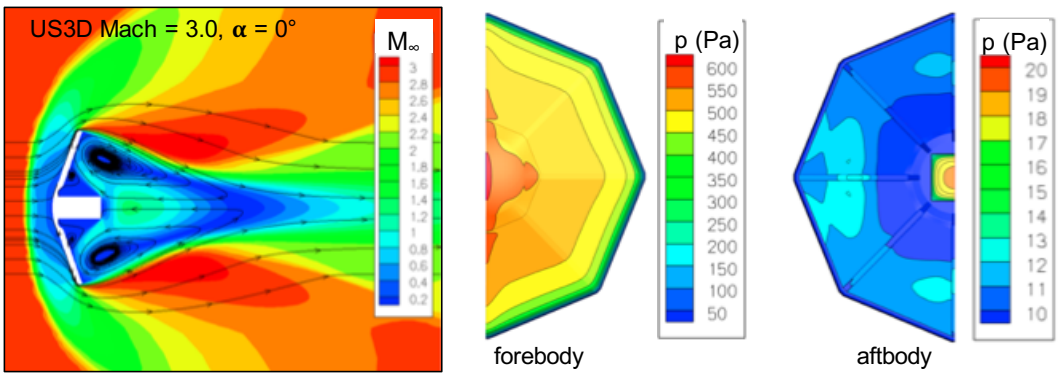

Fig. 8 Freestream Mach number contours and forebody surface pressure contours for Mach 3.0 conditions.

2. Transonic / Subsonic Static Aerodynamics CFD Simulation Approach

Transonic and subsonic static aerodynamics were generated with the Fully Unstructured Navier-Stokes (FUN3D) CFD code [12, 13]. FUN3D is a NASA-developed suite of tools for solving fluid dynamics problems using fully unstructured and mixed element grid topologies. FUN3D is regularly applied to subsonic, transonic, and supersonic aerodynamics simulations for blunt bodies, with and without backshells, and the same best practices developed for similar flight projects were applied in this analysis. FUN3D is capable of solving the Reynolds-Averaged Navier-Stokes equations through perfect gas and finite-rate simulations with included feature-based and adjoint-based mesh adaption. Local time-stepping is applied for steady flows, and second-order time-accuracy is applied for unsteady flows. The flow solver is based on second-order, node-based, finite-volume discretization. For the cases presented here, Roe?s flux reconstruction was used with no limiter. Solutions assumed perfect-gas air. The flow was modeled as fully turbulent using detached eddy simulation (DES) with a Spalart-Allmaras submodel and no compressibility correction. All solutions were run with 2nd order time-accuracy. Solutions were deemed to be complete once averaging of C_A over 5000 time step intervals resulted in less than a 3% change in coefficient value.

The computational grid for FUN3D was generated on a simplified geometry that eliminated the ribs and struts on the aft side of the heatshield and used a smooth, solid 3U CubeSat payload. These simplifications should not affect the static aerodynamics. Grids were full 3D and generated using AFLR3 and used an inviscid, tetrahedral mesh in the volume and prisms in the boundary layer near the body. The computational grids for this analysis average 9.8 million grid nodes. Wall spacing was determined to yield $y+$ values < 1 over the entire vehicle. The geometry, as well as a sample grid, from the FUN3D solutions is shown in Fig. 9.

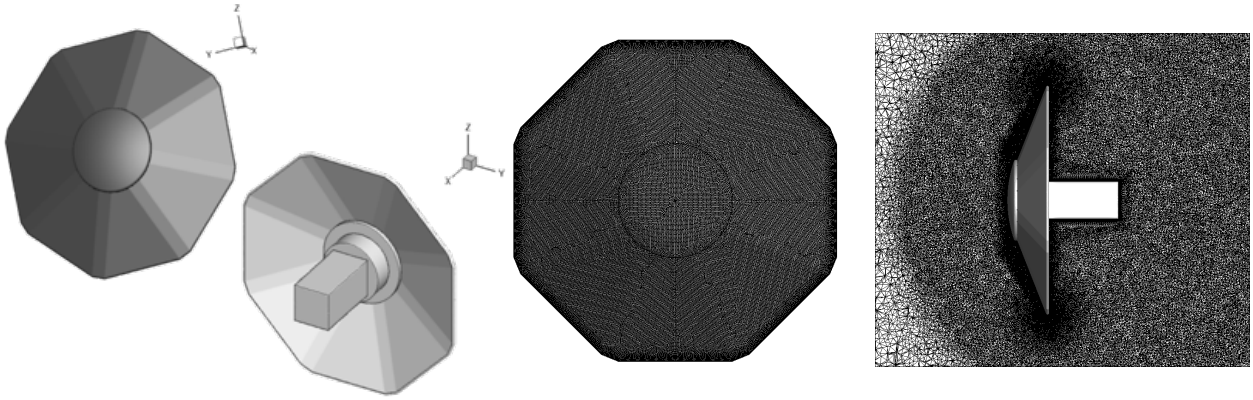

Fig. 9 FUN3D geometry and sample unstructured grid.

Figure 10 shows instantaneous velocity contours at Mach 0.3 and Mach 0.6 conditions with the vehicle at 0° angle of attack, zoomed to show the near-body flowfield. As expected, the flow separates around the shoulder of the vehicle, and the blunt body wake flow is unsteady. Similar to the supersonic CFD solutions, the aftbody pressures are appreciably lower than the forebody pressures, with the heatshield pressures dominating the resulting static aerodynamics.

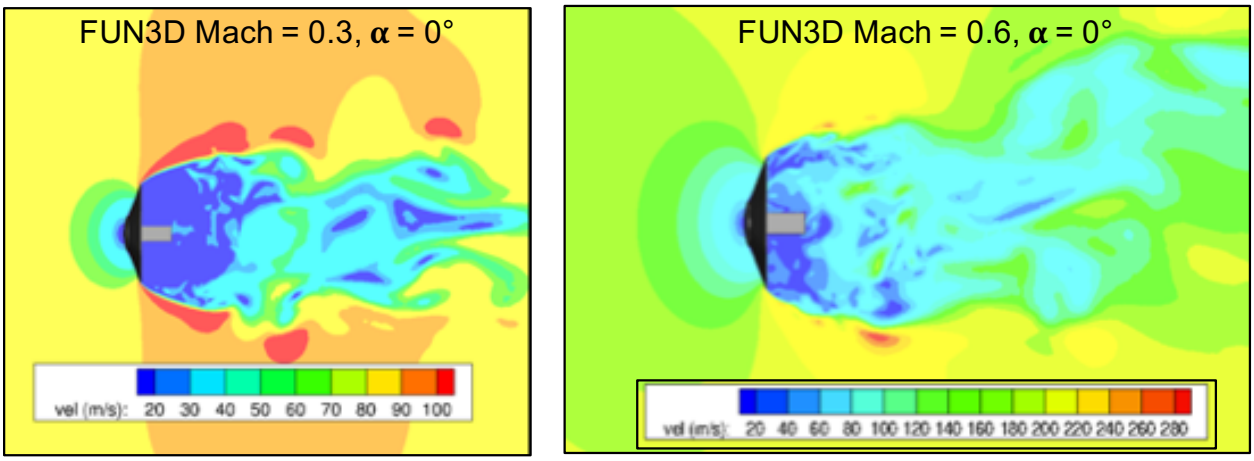

Fig. 10 Instantaneous velocity contours for Mach 0.3 (left) and Mach 0.6 (right) conditions and $\alpha = 0°$ (FUN3D).

C. Dynamic Pitch Damping

Blunt bodies are known to be dynamically unstable at supersonic Mach numbers, characterized by attitude growth during flight through these conditions [16]. A limited set of ballistic range shots (5 total) were conducted for ADEPT SR-1. While the data were useful to qualitatively evaluate the dynamic damping behavior of this shape, it was insufficient to develop a quantitative model. For ADEPT SR-1, functional forms developed from ballistic range testing for IRVE-3 [4] were implemented into the ADB to model dynamic damping. For dynamic pitch damping, aft geometry is a significant contributor to the driving mechanism that arises from unsteady variations in the aft body pressure distribution. While IRVE-3 was a 60° sphere-cone, it had a similar aft geometry with no backshell and an exposed payload extending aft from the nose (see Fig. 2). The axial CG position for ADEPT SR-1 (x_{CG}/D = -0.15) is forward of that from IRVE-3 ballistic range testing (x_{CG}/D = -0.23), but no damping data for similar shapes with further forward axial CG positions are known. At conditions where no data exist, the vehicle was assumed to be neutrally stable ($C_{m_q} = C_{n_r} = 0$).

D. Aerodynamics Uncertainties

Entry system performance was evaluated using Monte Carlo simulations with the Program to Optimize Simulated Trajectories II (POST2) [17, 18]. As part of this analysis, the nominal aerodynamics data uncertainties were provided by the ADB. Aerodynamics uncertainties for ADEPT SR-1 were largely based on past flight experience and engineering judgement from HIAD/IRVE missions. Table 3 shows the aerodynamics uncertainties applied for ADEPT SR-1. All uncertainties were applied uncorrelated, with the distributions listed in Table 3.

Aerodynamics uncertainties are typically larger at supersonic conditions compared to hypersonic (Mach >> 3), due to the challenges of modeling the separated wake and resulting contributions. Similar to IRVE-3, pitching and yawing moment uncertainties were modeled with both an adder term (shifts trim angle) and a multiplier term (changes moment slope). While ADEPT SR-1 was intended to be spin-stabilized, the moment uncertainty formulation was maintained to capture possible asymmetric shape changes, and a rolling moment uncertainty was included to account for limitations in the axisymmetric assumption. All moments were dispersed about the CG.

Table 3 Aerodynamics uncertainties for ADEPT SR-1

	Flight Regime	C_A	C_N	C_Y	C_{ll}	C_m	C_n	Distribution
Statics	Non-continuum	±5%	± 20%	± 20%		± 20%	± 20%	Normal
	Kn > 1000.0		± 0.01	± 0.01	1.24×10^{-6}	± 0.005	± 0.005	
Statics	Hypersonic	±3%	± 20%	± 20%		± 20%	± 20%	Normal
	M_∞ > 10		± 0.01	± 0.01	1.24×10^{-6}	± 0.003	± 0.003	
Statics	Supersonic	±10%	± 20%	± 20%		± 20%	± 20%	Normal
	M_∞ < 5		± 0.01	± 0.01	1.24×10^{-6}	± 0.005	± 0.005	

	Flight Regime	C_{m_q}	C_{n_r}	Distribution
Dynamics	Hypersonic	± 0.15	± 0.15	Uniform
	M_∞ > 6			
Dynamics	Supersonic	+0.4 × [2.0, 0.5] -	+0.4 × [2.0, 0.5] -	Uniform
	M_∞ < 3	0.4 + [0.1, 0.0]	0.4 + [0.1, 0.0]	

III. Results and Discussion

The following sections describe the static and dynamic aerodynamics database and flight performance of ADEPT SR-1. The aerodynamics database was implemented into the POST trajectory simulation as a standalone subroutine with inputs of Knudsen number, Mach number, angle of attack, and angle of sideslip. The ADB returns nominal aerodynamic force and moment coefficients in the body frame (Fig. 5). For off-nominal cases, the ADB accepts an array of dispersion parameters for coefficient and flight regime as inputs and returns dispersed aerodynamic force and moment coefficients.

A. Static Aerodynamics Database

As discussed in Section II, the static aerodynamics database was divided by flight regime. In the following figures, C_N and C_m are given in the α_T plane. The ADB decomposes these coefficients into the α and β planes (Fig. 5). Figure 11 shows the non-continuum aerodynamics for ADEPT SR-1, where decreasing altitude corresponds to decreasing Kn. At non-continuum conditions, large values of C_A and C_N, such as those plotted in Fig. 11, are common for blunt body entry vehicle shapes.

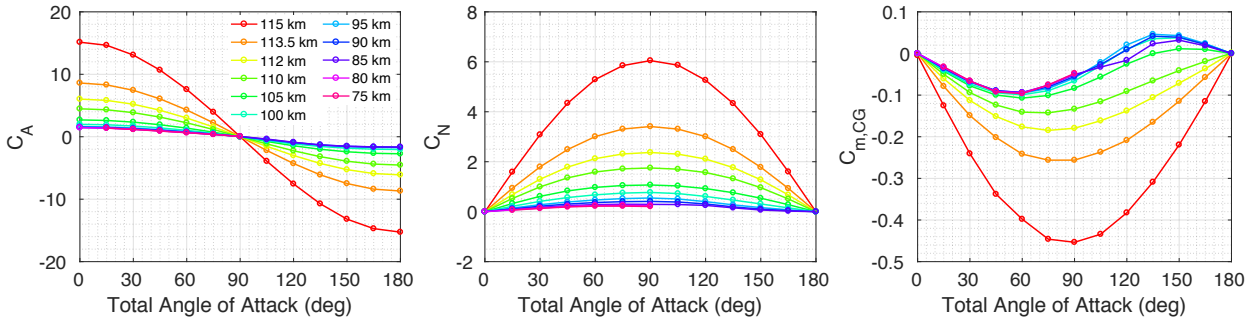

Fig. 11 Nominal non-continuum static aerodynamics (α_T plane).

Figure 12 shows the nominal continuum static aerodynamics database. The error bars in Fig. 12 are the ± 3σ values computed from the amplitude variation in the time-averaged CFD solutions. Figure 13 shows the same data, focused on conditions below Mach 1. The apparent discontinuity in force and moment coefficients at Mach 3.2 is the result of scaling the velocity to conditions away from design trajectory.

With no wind tunnel test data available on the faceted ADEPT SR-1 shape for comparison, comparisons with ground test data were limited to configurations with smooth sphere-cone forebodies. For C_A, the CFD results on the ADEPT SR-1 shape are lower than coefficient values derived from force balance data in supersonic wind tunnel testing of a

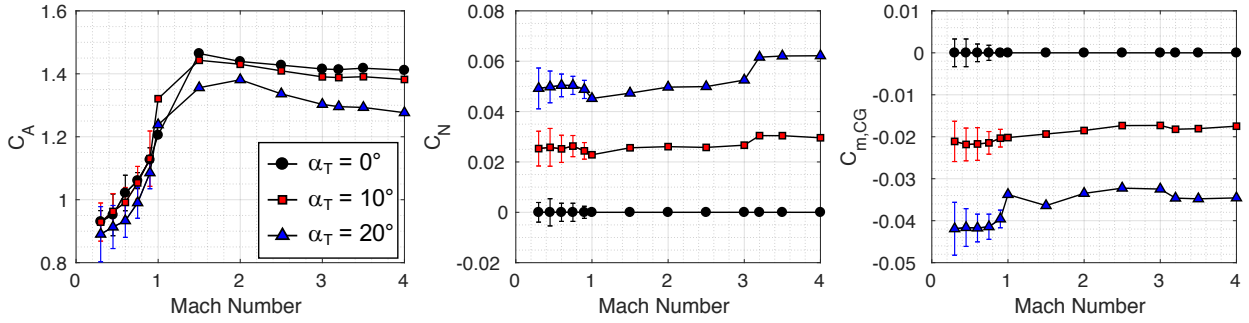

Fig. 12 Nominal continuum static aerodynamics (α_T plane).

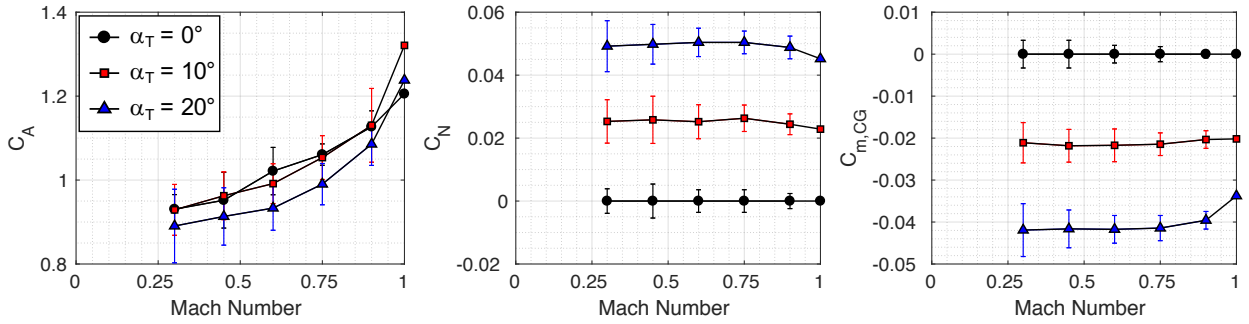

Fig. 13 Nominal subsonic static aerodynamics (α_T plane).

smooth 70° sphere-cone forebody [19]. Reynolds number differences are significant, as supersonic wind tunnel testing is generally on the order of Re_∞/ft = 1.0 million, while supersonic conditions along the ADEPT SR-1 design trajectory have Re_∞/ft between 0.15 and 0.35 million. Differences are also due to the ADEPT SR-1 shape having a smaller physical drag area than the smooth sphere-cone while both shapes use a reference area based on the circular projected area based on maximum diameter.

For blunt bodies, C_A dominates the static aerodynamics. As the vehicle decelerates, C_A decreases continuously from rarefied to continuum conditions. As the vehicle decelerates further, to supersonic conditions, the pressure coefficient on the aft surfaces decreases, providing a positive increment to the forebody axial force. This aft pressure contribution produces the slight rise in C_A shown prior to the sharp decrease through transonic conditions. As expected, at supersonic and subsonic conditions, C_N is at least an order of magnitude smaller than C_A, producing a negligible impact on the vehicle's static aerodynamic behavior. Pitching moment trends with angle of attack indicate the ADEPT SR-1 vehicle to be statically stable across the entire trajectory, for angles of attack below 20°.

B. Dynamic Damping Database

The dynamic damping database for ADEPT SR-1 was taken directly from IRVE-3 [4]. The ADB used functional forms derived from IRVE-3 ballistic range testing to yield C_{m_q} values as a function of Mach number and total angle of attack, with the assumption that the vehicle is axisymmetric ($C_{m_q} = C_{n_r}$). At non-continuum conditions, a constant, stable value of -0.32 is applied, from IRVE-3. At continuum conditions above Mach 3.5 in the ADB, Newtonian aerodynamic predictions of stable hypersonic pitch damping were blended with unstable supersonic pitch damping. Figure 14 shows the supersonic and subsonic dynamic damping database as functions of total angle of attack and Mach number. $C_{m_q} > 0$ is unstable, $C_{m_q} < 0$ is stable, and $C_{m_q} = 0$ is neutrally stable. Shapes like IRVE-3 are dynamically unstable at small angles of attack and Mach numbers below 2. In Fig. 14, the IRVE-3 dynamic damping model bounds the limited available data for the ADEPT geometry.

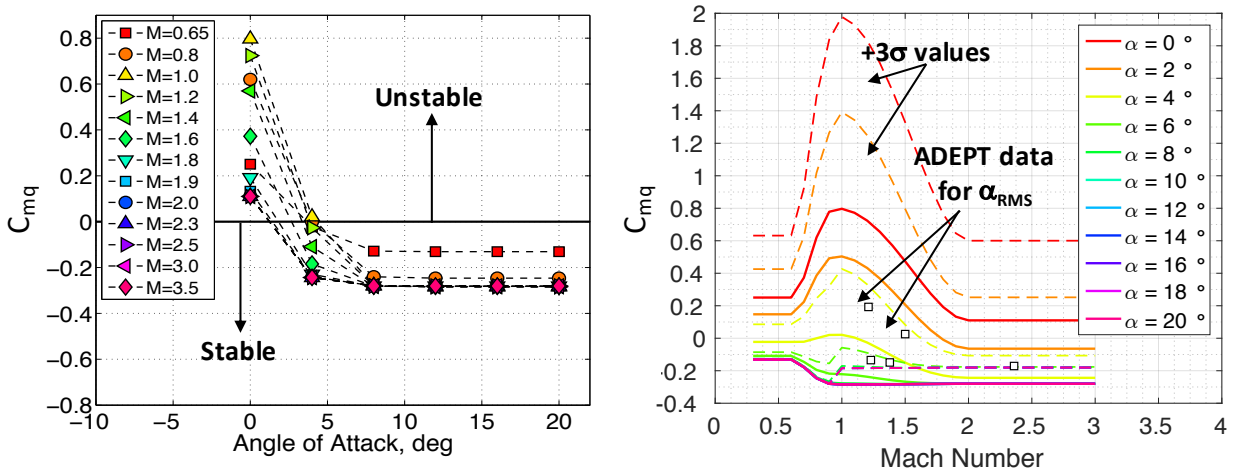

Fig. 14 Dynamic damping database.

C. Flight Performance

Vehicle aerodynamic force and moment coefficients for ADEPT SR-1 were calculated from linear and angular accelerations measured in flight with the AVA inertial measurement unit (IMU), reconstructed dynamic pressure, vehicle mass, reference area, and reference length. Post-flight reconstruction and trajectory simulation for ADEPT SR-1 are discussed in detail in [18, 20]. Atmosphere reconstruction was completed using balloonsonde measurements and GEOS-5 atmospheric model data reanalyzed with Earth-based observations on the day of launch [20]. The reconstructed aerodynamics were reconciled with the pre-flight ADB using a parameter estimation technique to solve for a set of dispersions that best fit the reconstructed trajectory. An equation error approach [21] was utilized to estimate parameters of the ADB that best fit the reconstructed force and moment coefficients. This approach has been used in the past for Mars Science Laboratory [22] and the Low-Density Supersonic Decelerator project [23]. The reconciled set of uncertainty factors were computed using a nonlinear least squares method to determine the best fit to the reconstructed total force and moment coefficients over the time period from 250-400 seconds after launch.

The aerodynamics were reconciled along the reconstructed trajectory shown in Fig. 15. Additional information on how the reconstructed trajectory was obtained from sensor data can be found in [20]. The attitude angles determined from reconstruction significantly exceed envelope of the pre-flight ADB after 350 seconds, resulting in extrapolation of force and moment coefficients for angles above 20°. These conditions occurred well past the pre-defined end of experiment at Mach 0.8.

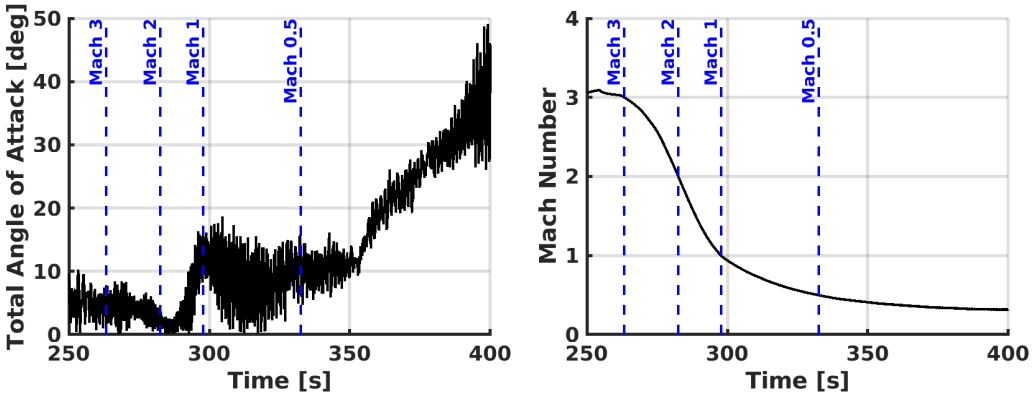

Fig. 15 Reconstructed trajectory.

The results of the parameter estimation approach are shown in Table 4. These parameters are the values of uncertainty factors determined to best fit the reconstructed aerodynamics and map to the supersonic/transonic/subsonic

uncertainties given in Table 3. Note that the uncertainty factors are normalized such that a value of unity corresponds to a 3σ uncertainty. As such, many of these values are well beyond the 3σ level. These results may be due to sensor misalignments that could corrupt side/normal and pitch/yaw adders in particular and will be investigated in future work.

Comparisons of the nominal, reconstructed, and reconciled aerodynamic force and moment coefficients are shown in Fig. 16. This figure shows the pre-flight nominal ADB along with the results of the reconstruction and best fit dispersed ADB given by the uncertainty factors listed in Table 4. Figure 17 provides a detailed view of the fits to the flight data over several oscillations for C_N and C_m. Axial force coefficient was under-predicted between 250 and 275 seconds, and the abrupt drop in C_A just before 300 seconds was not captured in pre-flight modeling. Past 275 seconds, axial force coefficient was over-predicted by the nominal ADB. Based on the parameter estimates given in Table 4, the reconstructed C_A was within the $\pm$ 3σ uncertainty on the nominal value.

The inaccuracy of the axisymmetric assumption for the ADEPT SR-1 shape is apparent in the comparisons of C_Y and C_N in Fig. 16, as these coefficient values are not centered about zero. The amplitude growth in pitch and yaw inherent in the C_Y and C_N histories was expected, due to the dynamic instability of blunt bodies decelerating through supersonic conditions. C_Y and C_N were under-predicted pre-flight, while C_m and C_n were over-predicted. In Table 4, the uncertainty parameter estimates for the pitch and yaw moment multipliers, which change the slope of the pitch and yaw stability curves, far exceed the 3σ values carried in the pre-flight ADB. It is expected that reformulation of the ADB as a function of both α and β, as opposed to α_T, will significantly reduce this discrepancy, as this will improve agreement of C_Y and C_N reconstructed in flight with values predicted through simulation at non-zero sideslip angles. If these updates do not significantly improve agreement with the reconstructed flight performance, wind tunnel testing is recommended to develop a ground test basis for aerodynamics of the faceted ADEPT shape.

Table 4 ADEPT SR-1 aerodynamic uncertainty parameter estimates

Uncertainty Factor	Value
Axial Force Multiplier	-0.7491
Normal Force Adder	2.7578
Normal Force Multiplier	-3.4816
Side Force Adder	3.8561
Side Force Multiplier	-3.2850
Pitch Moment Adder	-0.1862
Pitch Moment Multiplier	2.3841
Yaw Moment Adder	-0.0682
Yaw Moment Multiplier	2.3140
Pitch/Yaw Damping Adder	0.0600
Pitch/Yaw Damping Multiplier	1.0841

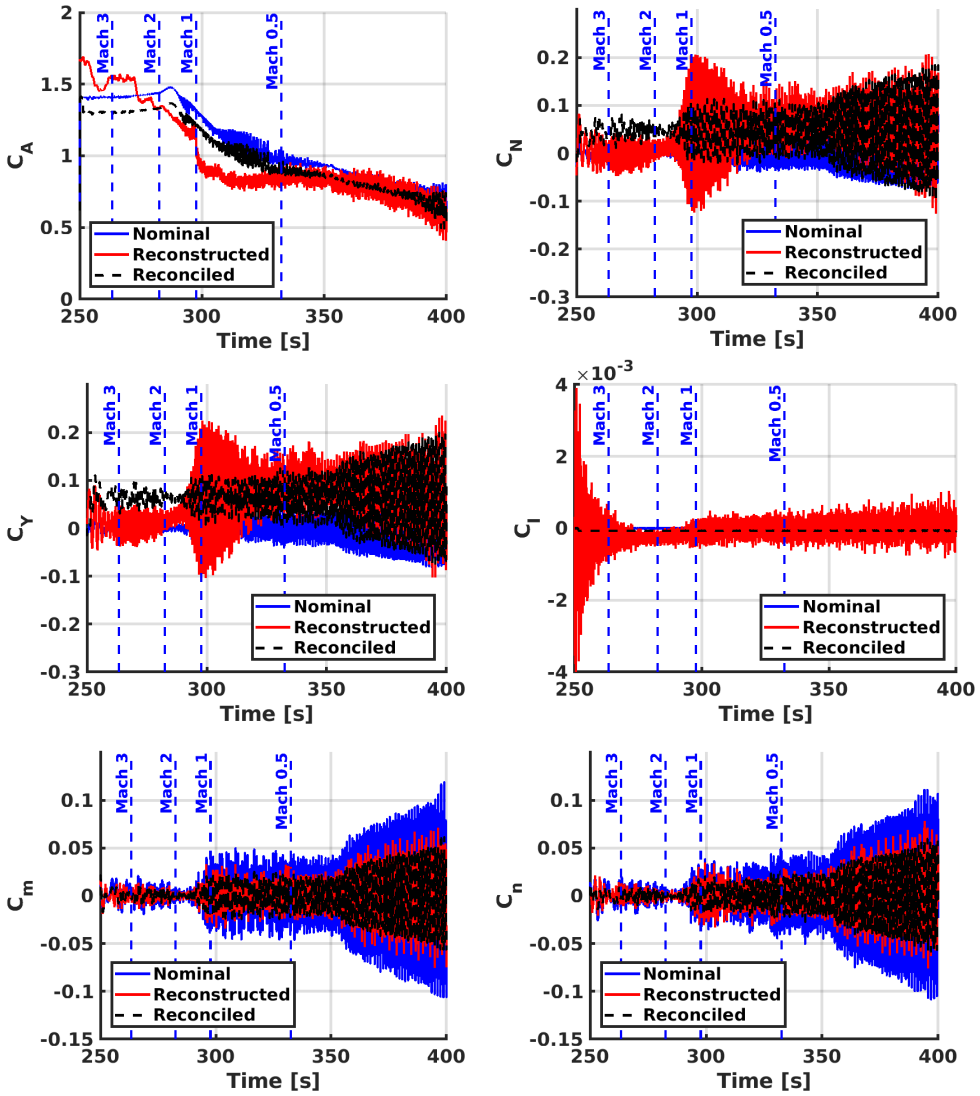

Fig. 16 Comparison of pre-flight nominal, reconstructed, and reconciled aerodynamic force and moment coefficients for ADEPT SR-1.

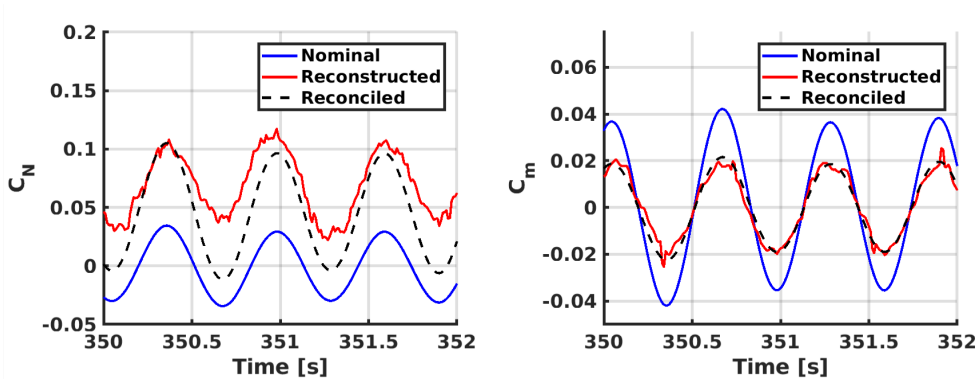

Fig. 17 Details of fits to ADEPT SR-1 flight data.

IV. Conclusions

ADEPT SR-1 successfully launched, deployed its heatshield above 100 km, and satisfied mission objectives to demonstrate deceleration without tumbling down to Mach 0.8 conditions. While the experiment was successful, reconstructed flight performance identified multiple limitations of the pre-flight aerodynamics database. Computational simulations were used to develop the entirety of the ADEPT SR-1 static aerodynamics database. For the supersonic, transonic, and subsonic conditions defining the ADEPT SR-1 trajectory, aftbody pressure is a significant contributor to the total axial force on the vehicle. Ground test data are generally used in place of CFD due to challenges of accurately modeling the effects of massively separated flow on pressure on such surfaces. During much of the ADEPT SR-1 flight, axial force coefficient was over-predicted, indicating a deficiency in the computational approaches used to simulate such conditions. Ground test data is necessary to reduce uncertainties in aerodynamics predictions for blunt bodies at supersonic, transonic, and subsonic conditions.

The ADEPT SR-1 shape is not axisymmetric but has eight, seamed fabric gores stretched across ribs, which are insufficient to approximate using a smooth conical surface. Aerodynamic reconstruction demonstrated the inaccuracy of the axisymmetric assumption, and forward work is expanding the aerodynamics database to account for effects arising from treatment of the heatshield as axisymmetric. At subsonic conditions, the vehicle experienced angles in excess of 20°, indicating a need to extend the aerodynamic database to larger angles. Additional work is also considering potential impacts of increased geometric detail in the computational grids, including the ribs, rib tips, seams, and payload structure.

Acknowledgments

The authors would like to acknowledge the NASA Flight Opportunities Program for support of ADEPT SR-1. The authors would also like to acknowledge contributions to this work from Derek Liechty, Karl Edquist, and Mark Schoenenberger at NASA Langley Research Center and Joseph Brock from Analytical Mechanics Associates at NASA Ames Research Center.

References

[1] Smith, B. P., Cassell, A. M., Kruger, C. E., Venkatapathy, E., Kazemba, C. D., and Simonis, K. R., "Nano-ADEPT: An Entry System for Secondary Payloads," IEEEAC Paper 7119095, March 2015.

[2] Wercinski, P. F., "ADEPT Sounding Rocket One (SR-1) Flight Experiment Overview," IEEEAC Paper 7943889, March 2017.

[3] O'Keefe, S. A., and Bose, D. M., "IRVE-II Post-Flight Trajectory Reconstruction," AIAA Paper 2010–7515, August 2010.

[4] Olds, A. D., Beck, R. E., Bose, D. M., White, J. P., Edquist, K. T., Hollis, B. R., Lindell, M. C., Cheatwood, F. M., Gsell, V. T., and Bowden, E. L., "IRVE-3 Post-Flight Reconstruction," AIAA Paper 2013–1390, March 2013.

[5] Moss, J. N., Glass, C. E., Hollis, B. R., and Norman, J. W. V., "Low-Density Aerodynamics for the Inflatable Reentry Vehicle Experiment," *Journal of Spacecraft and Rockets*, Vol. 43, No. 6, 2006, pp. 1191–1201.

[6] Schoenenberger, M., Cheatwood, F. M., and Desai, P. N., "Static Aerodynamics of the Mars Exploration Rover Entry Capsule," AIAA Paper 2005–0056, January 2005.

[7] Edquist, K. T., Desai, P. N., and Schoenenberger, M., "Aerodynamics for Mars Phoenix Entry Capsule," *Journal of Spacecraft and Rockets*, Vol. 48, No. 5, 2011, pp. 713–726.

[8] Lebeau, G. J., and Lumkin, F. E., "Application Highlights of the DSMC Analysis Code (DAC) Software for Simulating Rarefied Flows," *Computer Methods in Applied Mechanics and Engineering*, Vol. 191, No. 6-7, 2001, pp. 595–609.

[9] Liechty, D., "Object Oriented/Data-Oriented Design of a Direct Simulation Monte Carlo Algorithm," *Journal of Spacecraft and Rockets*, Vol. 52, No. 6, 2015, pp. 1521–1529.

[10] Nompelis, I. N., Drayna, T., and Candler, G. V., "A Parallel Unstructured Implicit Solver for Hypersonic Reacting Flow Simulations," AIAA Paper 2005–4867, June 2005.

[11] Nompelis, I. N., Drayna, T., and Candler, G. V., "Development of a Hybrid Unstructured Implicit Solver for the Simulation of Reacting Flows Over Complex Geometries," AIAA Paper 2004–2227, June 2004.

[12] Biedron, R. T., Carlson, J.-R., Derlaga, J. M., Gnoffo, P. A., Hammond, D. P., Jones, W. T., Kleb, W. T., Lee-Rausch, E. M., Nielsen, E. J., Park, M. A., Rumsey, C. L., Thomas, J. L., and Wood, W. A., "FUN3D Manual: 13.2," NASA TM 2017–219661, August 2017.

[13] Anderson, W. K., and Bonhaus, D. L., "An Implicit Upwind Algorithm for Computing Turbulent Flows on Unstructured Grids," *Computers and Fluids*, Vol. 23, No. 1, 1994, pp. 1–21.

[14] Smith, B. P., Yount, B., Kruger, C., Brivkalns, C., Makino, A., Cassell, A., Zarchi, K., McDaniel, R., Ross, J., Wercinski, P., Venkatapathy, E., Swanson, G., and Gold, N., "Nano-ADEPT Aeroloads Wind Tunnel Test," IEEEAC Paper 7500719, March 2016.

[15] Wright, M. J., Candler, G. V., and Bose, D., "A Data-Parallel Line Relaxation Method for the Navier-Stokes Equations," *AIAA Journal*, Vol. 36, No. 9, 1998, pp. 1603–1609.

[16] Kazemba, C. D., Braun, R. D., Schoenenberger, M., and Clark, I. G., "Dynamic Stability Analysis of Blunt-Body Entry Vehicles Using Time-Lagged Aftbody Pitching Moments," *Journal of Spacecraft and Rockets*, Vol. 52, No. 2, 2015, pp. 393–403.

[17] Striepe, S., Powell, R., Desai, P., Queen, E., Way, D., Prince, J., Cianciolo, A., Davis, J., Litton, D., Maddock, R., Shidner, J., Winski, R., O'Keefe, S., Bowes, A., Aguirre, J., Garrison, C., Hoffman, J., Olds, A., Dutta, S., Zumwalt, C., White, J., Brauer, G., Marsh, S., and Engel, M., *Program To Optimize Simulated Trajectories II (POST2), Vol. II: Utilization Manual,* Version 3.0.NESC, 2015.

[18] Dutta, S., and Green, J. S., "Flight Mechanics Modeling and Post Flight Analysis of ADEPT SR-1," AIAA Paper 2019–XXXX, January 2019.

[19] Korzun, A. M., Murphy, K. J., and Edquist, K. T., "Supersonic Aerodynamic Characteristics of Blunt Body Trim Tab Configurations," AIAA Paper 2013–2809, June 2013.

[20] Tynis, J. A., and Karlgaard, C. D., "Reconstruction of the Adaptable Deployable Entry and Placement Technology Sounding Rocket One Flight Test," AIAA Paper 2019–XXXX, January 2019.

[21] Morelli, E. A., and Klein, V., *Aircraft System Identification: Theory and Practice, Second Edition*, AIAA Education Series, Sunflyte Enterprises, Williamsburg, 2016, pp. 273–278.

[22] Schoenenberger, M., Norman, J. W. V., Karlgaard, C. D., Kutty, P., and Way, D. W., "Assessment of the Reconstructed Aerodynamics of the Mars Science Laboratory Entry Vehicle," *Journal of Spacecraft and Rockets*, Vol. 51, No. 4, 2014, pp. 1076–1093.

[23] Karlgaard, C. D., Kutty, P., O'Farrell, C., Blood, E., Ginn, J., and Schoenenberger, M., "Reconstruction of Atmosphere, Trajectory, and Aerodynamics for the Low-Density Supersonic Decelerator Project Aerodynamics of the Mars Science Laboratory Entry Vehicle (accepted)," *Journal of Spacecraft and Rockets*, Vol. TBD, No. TBD, 2019, p. TBD. doi:10.2514/1.A34223.